

EXPERIMENTAL INVESTIGATION OF THREE DIMENSIONAL SEPARATION BUBBLES

Andreas Krehmeller

e-mail: andreask@email.arizona.edu 

Mechanical engineering, Galgenbergstr. 30, D-93053 Regensburg - Germany, Head: Prof. Dr.-Ing. Stephan Lämmlein
Thesis conducted at the Hydrodynamics Laboratory at the Department of Aerospace and Mechanical Engineering at The University of Arizona - USA
Faculty advisor: Prof. Dr. Hermann F.asel

1. Introduction

Three dimensional laminar separation bubbles generated by a three dimensional adverse pressure gradient were investigated in experiments in a closed surface water tunnel for a Reynolds number range of $Re = 3,333$ to $Re = 7,500$. The pressure gradient was induced by an axisymmetric three dimensional displacement body (Fig 1.). The Reynolds number was based on the displacement body diameter with $d = 10$ cm.

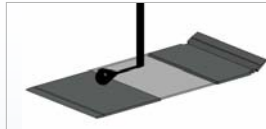


Fig 1. Concept of 3D displacement body and three segment modular flat plate.

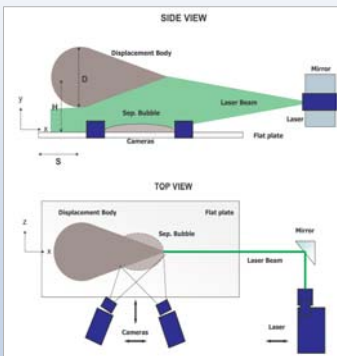


Fig 2. Sketch of the setup showing the displacement body and the separation bubble (not to scale). Also shown is the PIV system.

To exclude complex curvature effects the separation bubble was generated on a flat plate. Moreover, boundary layer suction was applied on the surface of the displacement body in order to prevent separation. Velocity vector field measurements with a Particle Image Velocimetry (PIV) system as well as dye flow visualization were employed for investigating the physical mechanisms governing the dynamics of the three dimensional separation bubble. First, the experiment was set up. This required the design and construction of the three dimensional displacement body, the flat plate, and a traverse system (Fig 2.). Then, experiments were carried out in the Hydrodynamics Laboratory at the University of Arizona.

2. Experimental Setup

The displacement body was built from a glass fiber shell. A negative mold was generated from a positive which was lathed from aluminium. In a second step the fiberglass positive was obtained (Fig 3.). Both, displacement body and flat plate were painted black to reduce glare. The suction holes have a diameter of $d_h = 1$ mm.



Fig 3. Design of the mould (left) and final displacement body (right).

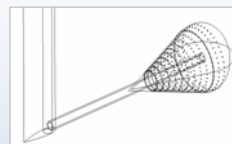


Fig 4. Displacement body illustrating the suction pipe and the attachment traverse.

The PIV system includes a double pulse YAG laser (class 4) and two high quality digital cameras. We designed and built a traverse system which can be moved with three stepper motors in x- and z-direction. The laser beam is pointed on a mirror which is inclined by 45° for generating a laser sheet with a thickness of approximately 2mm parallel to the side windows of the water tunnel.

Suction was generated through a long pipe leading to the basement. This method was preferred over a suction pump which may introduce undesired disturbances. The maximal achievable suction volume flow rate was 10.5 l/min. By adjusting the length of the suction pipe the flow rate could be either increased or decreased (Fig 4.). This adjustment was performed whenever the flow conditions (e.g. different Reynolds numbers) or the displacement body distance from the flat plate were altered.



Fig 5. Setup configuration of the PIV system with traverse and stepper motors.

We are using a stepper motor moving the laser in x-direction. This allows us to change the position of the laser sheet in the z-direction (Fig 5.). As a result the entire volume of the three dimensional separation bubble can be mapped out in fine slices.

3. Experiments

Boundary Layer suction has to be applied on the surface of the displacement body to diminish separation and to enhance the effect induced by the adverse pressure gradient. We took great care to assure that the boundary layer suction was as axisymmetric as possible (Fig 6.).

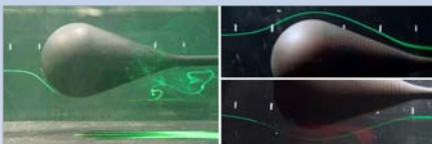


Fig 6. Flow visualization of the displacement body without (left) and with (right) boundary layer suction switched on at $Re = 7,500$, $H = D$ and $S = 2.5 D$.

Depending on the Reynolds number the bubble may be shedding in an unsteady fashion or for low enough Reynolds numbers reattach without unsteadiness. The topology of the bubble can be outlined by streamlines in the symmetry plane and by surface skin friction lines. The best flow visualization results were obtained when injecting the fluorescent dye through four holes on the surface of the flat plate slightly upstream of the developing separation bubble (Fig 7.). For high enough Reynolds numbers the Kelvin-Helmholtz instability results in a disturbance growth of the shear layer associated with the separation and the shedding of flow structures which can be seen in Fig 8. In addition, according to linear stability theory (LST) the growth rate of unstable disturbances waves are higher and the flow structures appear earlier leading to an earlier reattachment of the separated flow.

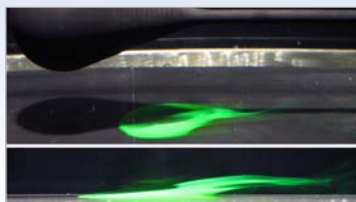


Fig 7. Perspective view (top) and sideview (bottom) of the three dimensional separation bubble using phosphorescent dye visualization at the baseline case ($Re = 7,500$, $H = D$, $S = 2.5 D$).



Fig 8. Sideview at $Re = 3,333$ (top) and $Re = 7,500$ (bottom) with $H = D$ and $S = 2.5 D$.

4. Results

By only visualizing the outer streamlines we were able to investigate the so called owl-face structures with its characteristic vortices in wall-normal direction as it was observed by e.g. Perry¹ (1986). Fig 9. compares a flow topology sketch from the literature with our flow visualization as well as results obtained from accompanied numerical calculations. The limiting streamlines are characterized by a saddle point (S) which is the upstream separation point in the symmetry plane as well as two foci (F) which are situated in the center of the owl-face structures.

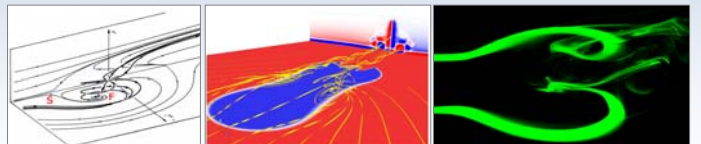


Fig 9. Owl-eyes development of the three dimensional separation bubble. Flow topology sketch (left) by Perry¹, numerical simulation (center) and dye flow visualization (right) for $Re = 3,333$, $H = D$ and $S = 3.5 D$.

The time-averaged velocity profiles of the separation bubble in the symmetry plane, shown in Fig 10. (top), depict the reverse flow region (recirculation zone). The magnitude of the reverse flow particularly in the upstream part of the bubble is much smaller than the freestream velocity. The velocity vectors are therefore barely visible. Nevertheless, the streamlines of the time-averaged flow in Fig 10. (bottom) clearly illustrate the reverse flow vortex.

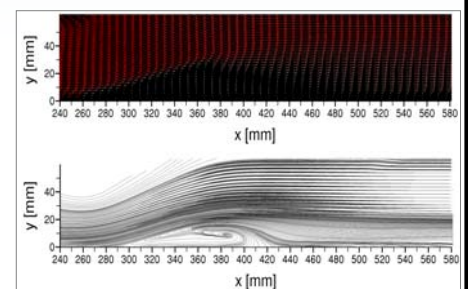


Fig 10. PIV data showing the time averaged velocity profiles (top) and the time averaged streamlines (bottom) at $Re = 7,500$, $H = D$ and $S = 2.5 D$.